



HAL
open science

Hemispherical sky radiance measurement using a fish-eye camera

Manchun Lei, Ewelina Rupnik, Jean-Pierre Papelard, Lâmân Lelégard, Olivier Martin, Jean-Philippe Souchon, Christophe Meynard

► **To cite this version:**

Manchun Lei, Ewelina Rupnik, Jean-Pierre Papelard, Lâmân Lelégard, Olivier Martin, et al.. Hemispherical sky radiance measurement using a fish-eye camera. Conférence Française de Photogrammétrie et de Télédétection (CFPT), Jun 2018, Champs-sur-Marne, France. hal-02555594

HAL Id: hal-02555594

<https://hal.science/hal-02555594>

Submitted on 27 Apr 2020

HAL is a multi-disciplinary open access archive for the deposit and dissemination of scientific research documents, whether they are published or not. The documents may come from teaching and research institutions in France or abroad, or from public or private research centers.

L'archive ouverte pluridisciplinaire **HAL**, est destinée au dépôt et à la diffusion de documents scientifiques de niveau recherche, publiés ou non, émanant des établissements d'enseignement et de recherche français ou étrangers, des laboratoires publics ou privés.

Hemispherical sky radiance measurement using a fish-eye camera

Manchun Lei, Ewelina Rupnik, Jean-Pierre Papelard, Lâman Lelégard,
Olivier Martin, Jean-Philippe Souchon, Christophe Meynard

LaSTIG MATIS, IGN, ENSG, Univ. Paris-Est 94160 Saint-Mandé, France

manchun.lei@ign.fr, ewelina.rupnik@ign.fr, jean-pierre.papelard@ign.fr,

aman.lelegard@ign.fr, olivier.martin@ign.fr, jean-philippe.souchon@ign.fr, christophe.meynard@ign.fr

Abstract

The objective of this work is to perform sky radiance angular distribution measurement using a fish-eye camera. The imaging system provides hemispherical high dynamic range (HDR) sky radiance images at high spatial resolution and radiometric sensibility, which can be used as complementary information for urban remote sensing application such as shaded surface reflectance retrieval. This communication presents the instrument, the radiometric and geometric calibration in detail.

1 Introduction

Solar radiation imaging systems have been developed for many years for various applications [1]–[6]. The system developed in [1] focused the relative variation of radiance and luminance distributions, the absolute radiance value was not used. Some others as [2], [3] were more interested in total irradiance value, which is the sum of pixels in the image, so the radiometric accuracy at each pixel was less demanding. In this work, our goal was to develop a system for measuring the hemispherical sky image in absolute radiance value using a fish-eye camera to improve the shaded surface irradiance estimation. The imaging system requires a good performance on radiometric response, vignetting correction and geometric calibration. The calibration process is similar to some previous works [4]–[6] but with different devices and methods. In this conference, the instrument, the calibration methods, the performance of the system and the result obtained will be presented.

2 Instrument description

The imaging system use an ultra-light smart camera CamLight [7], developed at the French Mapping Agency (IGN), which contains a 36 x 24 mm, 5120 x 3840 pixel CMOSIS CVM2000 sensor and a Xilinx Zynq-7030. The CMOS sensor is advantageous to avoid blooming and smearing effect compared to CCD sensor. The CamLight is controlled by Zynq-7030, a system on chip (SoC) + FPGA based on ARM cortex A9 running Linux OS and can be connected to the computer with Wi-Fi or Gigabit Ethernet interface. The CamLight can perform the acquisition sequence with different exposure times for HDR capture. The minimum exposure time is 100 μ s with a step of 1 μ s, which is important for measuring the circumsolar region. The raw images are stored in 12 bits for providing a good dynamic range.

3 Calibration method and results

The calibration process of the camera consists of geometric calibration and radiometric calibration.

Geometric calibration includes intrinsic calibration and *in-situ* calibration. The objective of intrinsic geometric calibration is to correct the distortion effect due to lens, to determine the direction of incident light of each pixel related to optical axis of camera. This calibration was performed using georeferenced ground control points (GCPs) (Figure 1) and the open-source software MicMac [8] before the sky image acquisition. *In-situ* calibration process determines the orientation of the optical axis related to the zenith and calculates the azimuth angle of the pixels. This calibration requires the geographical position of the camera and some points as reference in the images.

The objective of the radiometric calibration is to determine the relationship between the radiance L ($\text{W}/\text{m}^2/\text{sr}$) of incident light measured by the sensor and its output response. The pixel value recorded by the sensor is a response of measured light, modeled as:

$$P_{i,j}(I_{i,j}, t) = r(I_{i,j} \cdot t) + d_{i,j}(t) \quad (1)$$

Where $P_{i,j}$ is the digital count at i, j pixel location. $I_{i,j}$ is the incident irradiance (W/m^2) on the pixel, t is the exposure time, r is the radiometric response function of sensor, $d_{i,j}$ is the dark response function at i, j pixel location.

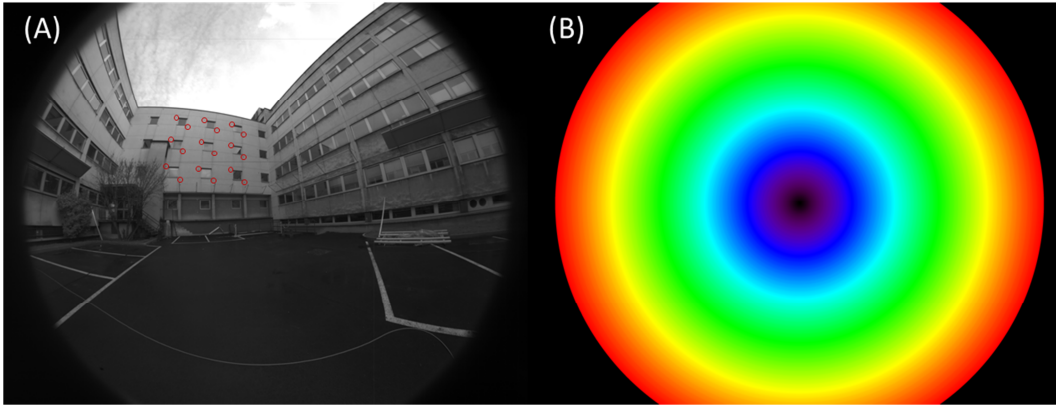


Figure 1. (A) An image contents GCPs (red circle) used for camera intrinsic geometric calibration, (B) Tilt angle related to optical axis, from 0° (black) to 90° (red), obtained by intrinsic calibration.

The irradiance on the pixel I is the product of incident radiance L , cosine of incident angle θ and the solid angle Ω :

$$I_{i,j} = L_{i,j} \cdot \cos(\theta_{i,j}) \cdot \Omega_{i,j} \quad (2)$$

That means for given incident radiance, the irradiance received on the pixel decreases from the optical center of image ($\theta = 0^\circ$) to the edge. This phenomenon is called vignetting effect. The vignetting effect is dependent on the characters of objective, especially focal distance and aperture diameter. For a given objective configuration, the vignetting can be described as a 2D model $V_{i,j}$, the relationship between irradiance received on the pixel and the incident radiance is described as:

$$I_{i,j} = V_{i,j} \cdot L_{i,j} \quad (3)$$

Dark response $d_{i,j}$ is the digital count recorded by camera without incident light. This response is provided by the current noise of sensor and related to the camera temperature. As the camera temperature increases with exposure time, dark response can be described as a function of t . The mean dark response values of CamLight's raw 12 bits images vary linearly from 15 to 115 at exposure times ranging from 1 ms to 100 ms. The dark corrected pixel value $P_{i,j}^d$ can be obtained:

$$P_{i,j}^d(I_{i,j}, t) = P_{i,j} - d_{i,j}(t) \quad (4)$$

The radiometric calibration determines the dark response function, vignetting model, and the radiometric response function in order to obtain the incident radiance from the camera measured digital count:

$$L_{i,j} = \frac{1}{t \cdot V_{i,j}} f(P_{i,j}^d) \quad (5)$$

Where $f = r^{-1}$, is a polynomial function.

In this work, the radiometric calibration was carried out mainly with a Labsphere integrating sphere and a Labsphere Unisource 600 lamp. To determine the coefficients of the polynomial, the camera was uniformly illuminated by Labsphere instruments with a constant radiance during measurements. The radiance of incident light was measured by an OceanOptic spectrometer and converted to CamLight band integral radiance L_{ref} ($\text{W}/\text{m}^2/\text{sr}$):

$$L_{ref} = \int L(\lambda)q(\lambda)d\lambda \quad (6)$$

Where $L(\lambda)$ is the spectral radiance ($\text{W}/\text{m}^2/\text{sr}/\text{nm}$) of incident light measured by spectrometer, $q(\lambda)$ is the quantum efficiency curve of sensor.

Images were acquired with various exposure times from 0.1 ms to 100 ms. The result of this calibration is shown in Figure 2 (A and B). We can notice that CamLight provides a very linear response. The dark corrected count values given in Figure 2 were determined by a 5 x 5 element average taken from the center of the image. The mean absolute percentage error (MAPE%) is 0.78%.

The vignetting model was determined by "flat-field" images acquired with a spherical light diffuser under opaque cloudy sky, illustrated in Figure 2 (C and D).

In Figure 3, 2 sky radiance images measured on 07 June 2018 are presented. These images provide the hemispherical downward sky radiance distribution with good radiometric and geometric accuracy.

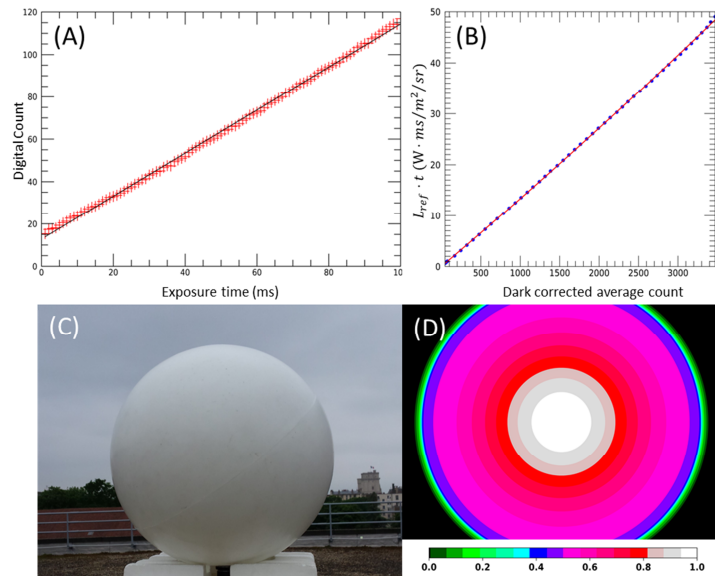


Figure 2. (A) Dark noise as a function of exposure time, (B) Linearity of radiometric response of the camera, (C) Measurement of flat-field image using spherical light diffuser under opaque cloudy sky, (D) Obtained vignetting map.

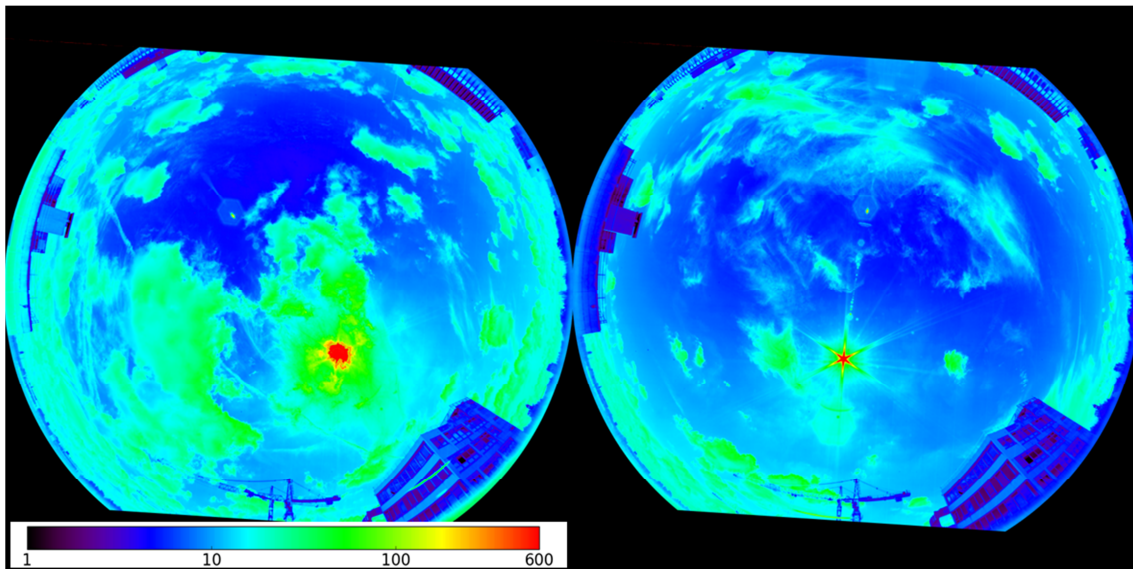


Figure 3, Sky radiance images measured on 07 June 2018, UTC 10:34 (left) and 12:05 (right).

References

- [1] E. G. Rossini and A. Krenzinger, "Maps of sky relative radiance and luminance distributions acquired with a monochromatic CCD camera," *Sol. Energy*, vol. 81, no. 11, pp. 1323–1332, 2007.
- [2] C. Gauchet, P. Blanc, B. Espinar, B. Charbonnier, and D. Demengel, "Surface solar irradiance estimation with low-cost fish-eye camera," in *Workshop on "Remote Sensing Measurements for Renewable Energy"*, 2012.
- [3] R. Chauvin, J. Nou, S. Thil, and S. Grieu, "Modelling the clear-sky intensity distribution using a sky imager," *Sol. Energy*, vol. 119, pp. 1–17, 2015.
- [4] K. J. Voss and G. Zibordi, "Radiometric and geometric calibration of a visible spectral electro-optic 'fisheye' camera radiance distribution system," *J. Atmospheric Ocean. Technol.*, vol. 6, no. 4, pp. 652–662, 1989.
- [5] R. Roman *et al.*, "Calibration of an all-sky camera for obtaining sky radiance at three wavelengths," 2012.
- [6] B. Urquhart, B. Kurtz, E. Dahlin, M. Ghonima, J. Shields, and J. Kleissl, "Development of a sky imaging system for short-term solar power forecasting," *Atmospheric Meas. Tech.*, vol. 8, no. 2, pp. 875–890, 2015.
- [7] O. Martin, C. Meynard, M. Pierrot Deseilligny, J.-P. Souchon, and C. Thom, "Réalisation d'une caméra photogrammétrique ultralégère et de haute résolution," in *Proceedings of the colloque drones et moyens légers aéroportés d'observation, Montpellier, France, 2014*, pp. 24–26.
- [8] E. Rupnik, M. Daakir, and M. P. Deseilligny, "MicMac—a free, open-source solution for photogrammetry," *Open Geospatial Data Softw. Stand.*, vol. 2, no. 1, p. 14, 2017.